Potential for early forecast of Moroccan wheat yields based on climatic drivers

Jascha Lehmann[1], Marlene Kretschmer[1], Bernhard Schauberger[1], and Frank Wechsung[2]

[1]Potsdam Institute for Climate Impact Research
[2]Potsdam-Institute for Climate Impact Research

November 22, 2022

Abstract

Wheat production plays an important role in Morocco with the country typically producing more than half of Northwest African grain production. Current wheat forecast systems use weather and vegetation data during the crop growing phase, thus limiting the earliest possible release date to early spring. However, Morocco's wheat production is mostly rainfed and thus strongly tied to fluctuations in rainfall, which in turn depend on slowly evolving climate dynamics. This offers a source of predictability at longer timescales. Using physically-guided causal discovery algorithms we extract climate precursors for wheat yield variabilityfrom gridded fields of geopotential height and sea surface temperatures which show potential for accurate yield forecasts already in December. The detected interactions are physically meaningful and consistent with documented ocean-atmosphere feedbacks. Reliable yield forecasts at such long lead times could provide farmers and policy-makers with necessary information for early action and strategic adaptation measurements to support food security.

Potential for early forecast of Moroccan wheat yields based on climatic drivers

J. Lehmann[1], M. Kretschmer[2], B. Schauberger[1], and F. Wechsung[1]

[1]Potsdam Institute for Climate Impact Research (PIK), Member of the Leibniz Association, Potsdam, Germany

[2]University of Reading, Reading, United Kingdom

Corresponding author: Jascha Lehmann (jlehmann@pik-potsdam.de)

Key Points:

- Moroccan wheat yield anomalies are hindcasted four months before harvest based on climate precursors.
- Precursors are extracted from gridded fields of climate variables using physically guided causal discovery algorithms.
- The detected causal interactions are physically meaningful and consistent with documented teleconnections in the climate system.

Abstract

Wheat production plays an important role in Morocco with the country typically producing more than half of Northwest African grain production. Current wheat forecast systems use weather and vegetation data during the crop growing phase, thus limiting the earliest possible release date to early spring. However, Morocco's wheat production is mostly rainfed and thus strongly tied to fluctuations in rainfall, which in turn depend on slowly evolving climate dynamics. This offers a source of predictability at longer timescales. Using physically-guided causal discovery algorithms we extract climate precursors for wheat yield variability from gridded fields of geopotential height and sea surface temperatures which show potential for accurate yield forecasts already in December. The detected interactions are physically meaningful and consistent with documented ocean-atmosphere feedbacks. Reliable yield forecasts at such long lead times could provide farmers and policy-makers with necessary information for early action and strategic adaptation measurements to support food security.

Plain Language Summary

The per capita consumption of cereals in Morocco is one of the highest in the world placing a significant role to wheat production in the framework of national food security. Early wheat forecasts are crucial to increase the resilience of the agricultural sector to climate risks. So far, operational forecast systems provide first yield estimates in March-April and hence around one month before harvest starts in May. These systems use weather and vegetation data during the crop growing phase thus limiting the earliest possible release date to this very time period. Here, we present a different approach based on causal interactions in the climate system to provide accurate forecasts of year-to-year wheat yield changes already in December. We make use of the fact that wheat production is mostly rainfed and thus strongly coupled to prevailing rain conditions which, in turn, are influenced by slowly evolving circulation patterns and sea surface temperatures in the Atlantic and Pacific Ocean. These links between far-away regions, also known as teleconnections, can last for several months and thus provide predictability at seasonal timescales relevant for strategic adaptation decisions, e.g. regarding crop import planning or the choice and intensity of agronomic practices.

1 Introduction

Agriculture is of particular strategic importance in Morocco. Most of the arable land is devoted to cereals with wheat accounting for the majority of total cereal production and thus playing a key factor for national food security. However, most of the arable land is located in arid or semi-arid regions which are characterized by long dry periods and high year-to-year rainfall variations (Born et al., 2008). Since very little of the arable land is irrigated, this leaves Morocco's wheat production heavily dependent on large fluctuations in rainfall intensities (Berdai et al., 2011). Reliable seasonal forecasts could help in reducing the vulnerability of the Moroccan agriculture to weather risks by enabling timely in-season adaptation. Since the Moroccan climate is projected to become drier and hotter with ongoing global warming, such forecasts will likely become even more important in the future (Born et al., 2008; Filahi et al., 2017).

Operational yield forecasting systems provide estimates at lead times of a few days up to three months before harvest in May-June. Provisional forecasts are released every year by the Crop Growth Monitoring System – Morocco (CGMC-MAROC) in April and then constantly revised over the course of the season. CGMS-MAROC uses a physical crop growth model combined with statistical models (Bernardi, 2016; Bregaglio et al., 2014). Based on empirical regression models using weather and vegetation data Balaghi et al. (2008) accurately forecast grain yields as early as of March. Yet, both approaches use the Normalized Difference Vegetation Index (NDVI) during mid-season of the growing phase which limits the earliest possible release date to early spring.

Longer lead times may be achieved through utilization of remote climatic drivers which influence rainfall variability over Morocco and thus wheat production. Total annual wheat yields are significantly correlated to accumulated rainfall during the rainy season lasting from September to May (De Wit et al., 2013). Intra-seasonal rainfall variability in turn is influenced by large-scale climate dynamics including atmospheric circulation patterns and sea surface temperatures over the Pacific and Atlantic Ocean which may persist over months allowing for skillful forecasts at extended lead times (Knippertz et al., 2003; Rodríguez-Fonseca et al., 2006). The most prominent mode of large-scale variability in the Atlantic, the North Atlantic Oscillation (NAO), has been shown to directly influence the early stage of Moroccan wheat growth in December by shaping the storm tracks which bring moist air from the Atlantic Ocean to the land (Jarlan et al., 2014). Moreover, indirect influences on Moroccan rainfall may occur via atmospheric teleconnections; wave trains, for instance, can emerge from sea surface temperature forcing and may lead to temperature and rainfall changes in far-away regions downstream of the wave (Schlueter et al., 2019; Shaman & Tziperman, 2011).

Tapping into this potential source of forecasting rainfall and thus Moroccan wheat yields, we here apply a physically motivated approach based on causal discovery algorithms (Runge et al., 2019) to find causal climate precursors for interannual wheat yield variability at least four months before harvest. Previous studies have successfully applied the methodology of causal precursors to forecast extreme stratospheric polar vortex states relevant for mid-latitude winter weather (Kretschmer et al., 2017) and the Indian summer monsoon intensity (Di Capua et al., 2019).

2 Data

Moroccan wheat yield (MWY) data. Nationally aggregated annual wheat yield data for the time period 1979-2017 is taken from the website of the Food and Agriculture Organization (FAO) (FAOSTAT, 2017) with wheat yields given in hectograms per hectare (hg/ha). Annual anomalies are calculated based on the difference to the yield in the previous year (first differences) thereby removing possible linear trends.

Climate data. Precursors are derived from two climate variables: sea surface temperature (SST) and geopotential height at 500 hPa (Z500), with the latter being a commonly used level to describe high and low pressure systems in the mid troposphere. We selected these climate variables because they were shown to be linked to Moroccan winter climate and/or wheat yields (e.g. Jarlan et al., 2014; Knippertz et al., 2003; Tuel & Eltahir, 2018). Both climate variables are taken from the ERA5 reanalysis product provided on a 1° x 1° longitude-latitude grid covering the time period 1979-2017 at monthly time resolution (Hersbach et al., 2019). Similarly, as for the MWY time series, monthly climate anomalies are calculated at each grid cell by calculating the difference to the same month of the previous year. Due to the first differences approach for anomaly calculation and the wheat growing season lasting from November to June, the analysis is limited to the years 1981-2017.

3 Building the statistical forecast model – a three step approach

Building the forecast model consists of three steps: (1) defining potential precursors from gridded climate variables by hierarchical clustering of correlation maps, (2) selecting causal precursors from potential precursors using causal discovery algorithms and (3) applying multiple-linear regressions on observed yield anomalies using causal precursor time series.

Step 1: Define potential precursors

Potential precursors are defined as confined regions of a climate variable whose changes precede changes in the target variable, i.e. nationally aggregated MWY anomalies. In a first step, pairwise correlation analyses are conducted between MWY anomalies and lagged time series of monthly Z500 and SST anomalies at each grid cell of the gridded globe between 90°N and 20°S to include possible teleconnections from the northern hemisphere and the tropics. Thereby, statistical significance at the grid cell level is defined at the 2% threshold (two-tailed p-value < 0.02). Using two climate variables (Z500 and SST) and four time lags (September to December) thus leads to eight correlation maps from which potential precursors are extracted. Potential precursors are defined by grouping significantly correlated grid cells of the same correlation sign using Density-Based Spatial Clustering of Applications with Noise (DBSCAN, Ester et al., 1996;

Schubert et al., 2017). In DBSCAN a radius of 300 km is chosen to define neighboring grid cells which is found to produce regions of reasonable sizes and spatial separation.

Step 2: Select causal precursors from potential precursors

So far potential precursor regions have been identified which are correlated with the target variable MWY. These lagged correlations, however, do not necessarily imply causation. Non-causal, spurious correlations can emerge from indirect links, common drivers or autocorrelation effects. To remove such spuriously correlated precursors we apply a multivariate causal discovery algorithm (Runge et al., 2019). The algorithm uses partial correlations to iteratively check whether the link between a given potential precursor and the target variable can be explained by any combination of the remaining potential precursors. If this is the case, i.e. if the given potential precursor is conditionally independent from the target variable, then this potential precursor is removed. Otherwise, it is considered as a causal precursor. A detailed step-by-step description of this causal selection step can be found in Kretschmer et al. (2016). Despite the thorough selection process the definition of causality given here, like any causal interpretation, rests on several underlying assumptions (J. Runge, 2018). In this sense, causal precursors as defined in this study should be understood as climatic indices which exhibit a significant, time-lagged linear dependence with MWY anomalies that cannot be explained by any other identified potential precursor or combination of those.

The combination of step 1 and step 2 of the method part was first introduced by Kretschmer et al. (2017) as the response-guided causal precursor detection. Here, we apply the same method albeit with the modification of clustering significantly correlated grid cells in step 1 in contrast to merging only directly neighboring grid cells. This has shown to improve the robustness of detecting potential precursor regions.

Step 3: Build the forecast model based on causal precursors

In the last step we perform a multiple-linear regression between the anomaly time series of the selected causal precursors and MWY anomalies to build the forecast model in the form $\mathrm{MWY}_{\mathrm{forecast}} = \alpha + \sum_{i}^{n} \beta_i \cdot \mathrm{CP}_i + \varepsilon_i$, where α is the intercept, β_i is the parameter of the i-th causal precursor (CP_i) with error term ε_i and n is the total number of causal precursors.

4 Results

4.1 Extracting causal precursors from climate data

In total 61 potential precursors are extracted (step 1) from the pairwise correlation analysis between the gridded climate variables and MWY anomalies indicating both positive as well as negative correlations (respective red and blue regions with contours in Fig. 1). Potential precursors are found in each correlation map with spatial patterns of Z500 precursors showing larger differences between time lags compared to SST as expected from higher variability in the

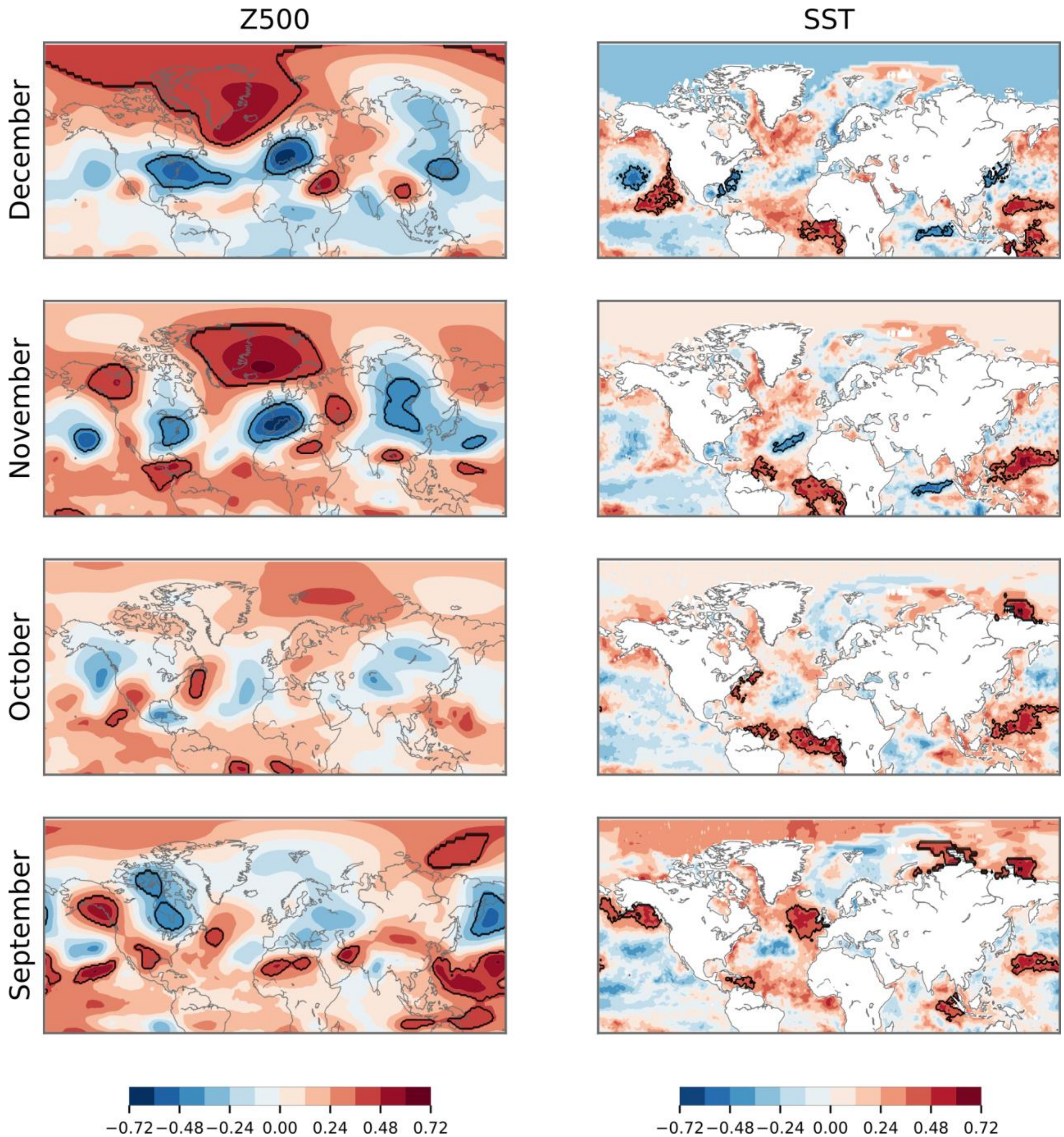

Fig. 1: Potential precursors derived from 500 hPa geopotential height anomaly fields (Z500, left) and sea surface temperature anomaly fields (SST, right). Pairwise correlations are calculated between wheat yield anomalies and the respective climate variable at each grid cell and time lag ranging from lag 4 (December) to lag 7 (September). Significantly correlated grid cells are then aggregated to homogeneous regions using cluster analysis (black contours).

atmosphere. Correlation maps are robust with similar regions found for different significance thresholds and subsamples of the studied time period (see details in Supporting Information (SI), Fig. S1).

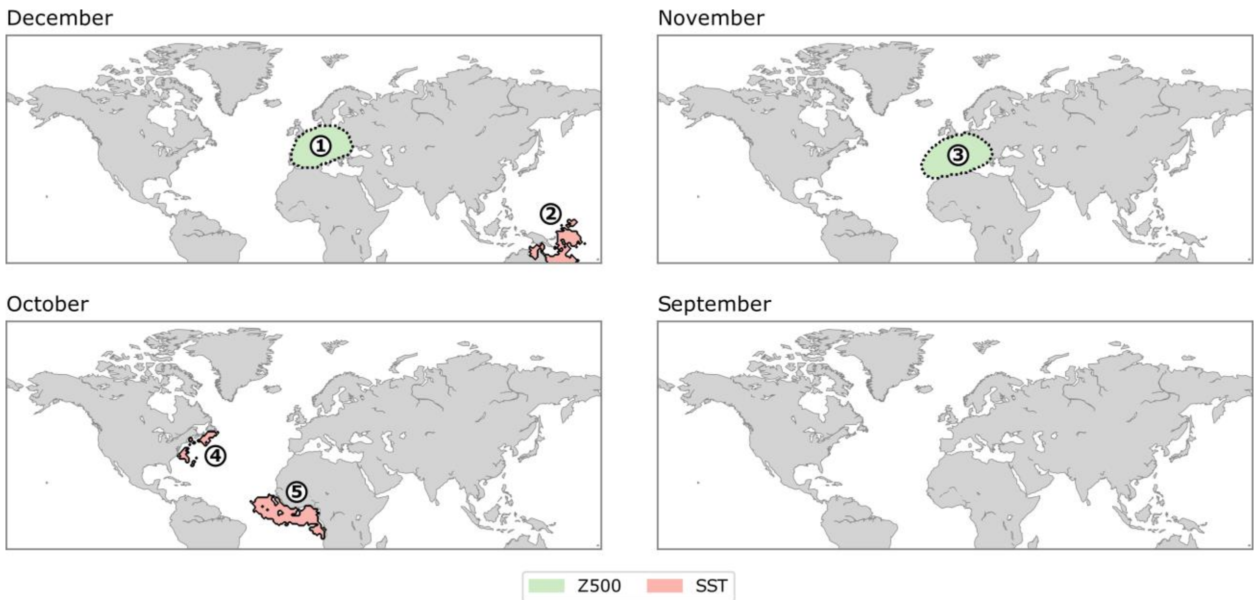

Fig. 2: Causal precursors of Moroccan wheat yield anomalies. Five causal precursor regions are extracted from geopotential height anomaly fields (Z500, green) and sea surface temperature anomalies (SST, red) at different time lags. Contours indicate whether a precursor is positively (solid line) or negatively (dotted line) correlated with yield anomalies.

Amongst all 61 potential precursors only five are found to be causally linked to WWY anomalies following step 2 of the model building approach (Fig. 2). These causal precursors include a region of negatively correlated Z500 anomalies over Central to Southwestern Europe in November and December suggesting that Z500 anomalies in these months provide relevant, independent information for MWY. Otherwise, the applied causal discovery algorithm should have eliminated one of the two precursors during the conditional independence test. Consistently, the correlation between both Z500 regions is only weak (Pearson correlation coefficient of r=0.36, Fig. S2). A second causal precursor is found in December which refers to positively correlated SST anomalies in the Coral Sea northwest of Australia. Two causal precursors emerge in October and relate to positively correlated SST anomaly fields – one in the North Atlantic off the East Cost of the USA and the other in the tropical Atlantic along the western African coastline. In September no causal precursor for MWY is identified.

We test the robustness of the causal selection step by altering significance thresholds and applying them to subsamples of the data and overall find consistent results (see detailed discussion in SI, Fig. S3). Particularly, causal precursors 1-4 only show little sensitivity to the chosen settings.

4.2 Validation of the Moroccan wheat yield hindcasts

Hindcasted yield anomalies strongly correlate with observed anomalies, explaining 88% of the observed yield variance over the full time period (Fig. 3a). Thereby, each causal precursor contributes a similar individual share of 15-25% to the total explained variance (Fig. S4) as computed from variance decomposition of the multiple-linear regression model (Grömping, 2007). Oscillating MWY variability over the last decade seems to be driven by similar variability of the causal Z500 precursor regions in December and November (Fig. S5) which is in line with an increased correlation strength over time between both precursors and MWY (Fig. S6). In contrast, correlation strength between MWY and the causal SST precursor in the equatorial Atlantic starts at a high level of around r=0.8 and then decreases to around r=0.4 in 2010. The transition phase when the correlation of MWY with the Z500 precursors becomes stronger than with the SST precursor corresponds to the time period where hindcasts diverge most from observations (1999-2003) and may thus play a role for this discrepancy. Analyses of the hindcast residuals confirm that the assumptions of a multiple-linear regression model are fulfilled; that is that residuals are characterized by a mean value of zero, constant variance (homoscedasticity), no significant auto-correlation and follow a normal distribution (Fig. S7).

The regression model is robust with respect to its regression parameters of the identified causal precursors. To show this we divide the time series into two parts; regression parameters are derived from the training period (19 years, 1981-1999) and then used to hindcast MWY anomalies over the test period (18 years, 2000-2017). The explained variance over the training period (91%) is high and similar to the explained variance over the test period (85%), indicating that the regression model does not suffer from overfitting given the hypothetical case that all five causal precursors were known (Fig. 3b).

We next implement an out-of-sample cross validation to further validate the predictive skill of our hindcast model in the case that causal precursors are not know a priori. For this, we iteratively remove two consecutive years from the time series with the remaining years serving as the training period and the left-out years as the test period. We choose to remove two consecutive years instead of just one to account for the strong year-to-year autocorrelation of the causal precursor time series (Fig. S8). The full hindcast model (step1-3) is then calculated using data from the training period only to ensure that data against which the model skill is validated does not enter any part of the model building process.

Hindcasted yield anomalies from this cross validation still explain 46% of the observed variance over the full time period with observations mostly staying within the 95% prediction interval (Fig. 3c). The drop in explained variance is due to the fact that not all five causal precursors are detected in each training period which is primarily due to small changes in the identified potential precursor sets. Repeating the cross-validation using prescribed potential precursors from the full time period increases the explained variance to 76% (Fig. S9).

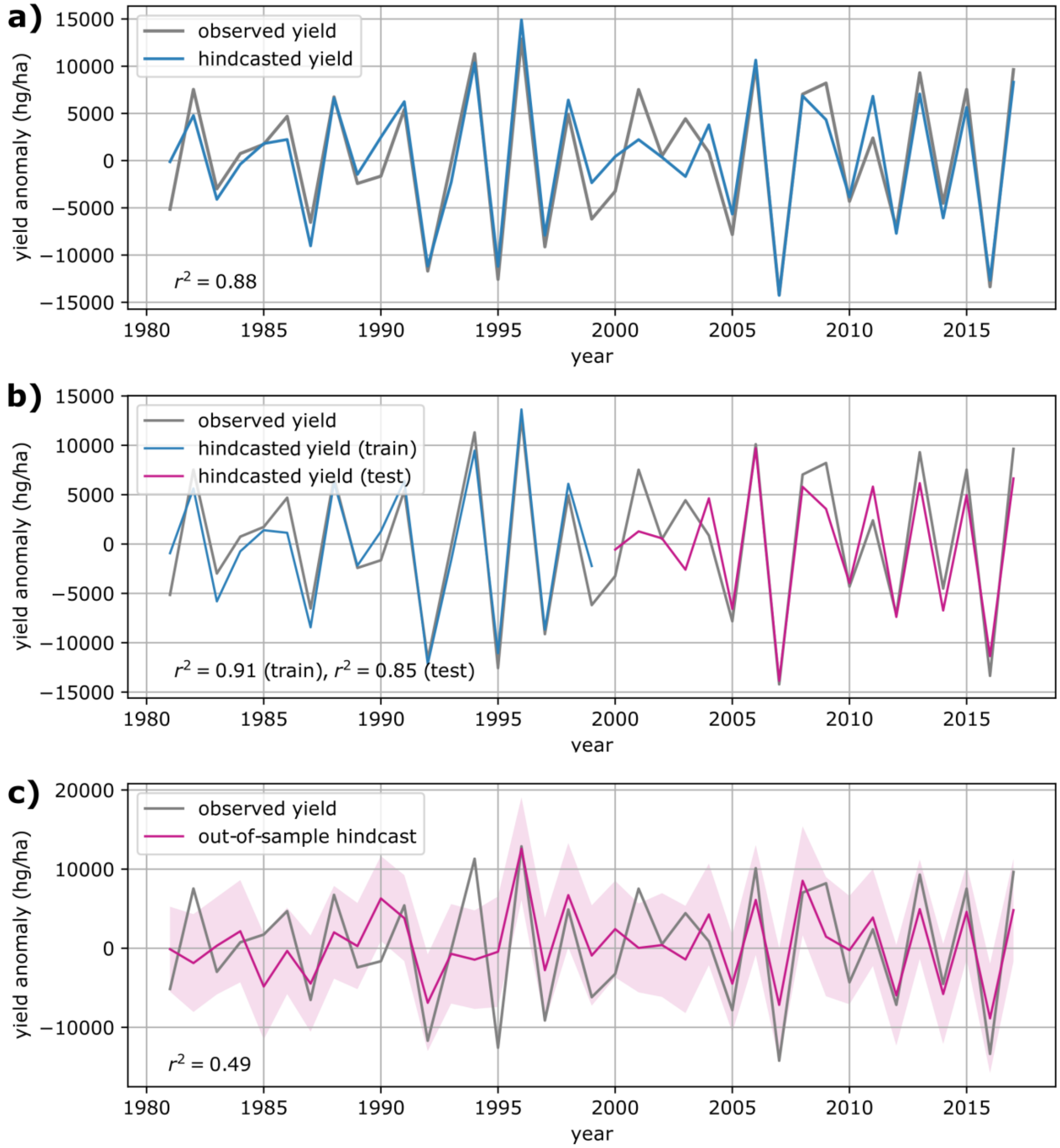

Fig. 3 Hindcasts based on causal precursors. (a) Hindcasted yields strongly correlate with observed yields over the studied time period. (b) Observed and hindcasted yields over a train and a test period with same causal precursors as in (a) and regression parameters calculated from the train period only. (c) Leave-2-out cross validation with strict train-test splitting for all three model building steps. Observed yields mostly stay within the 95% prediction interval.

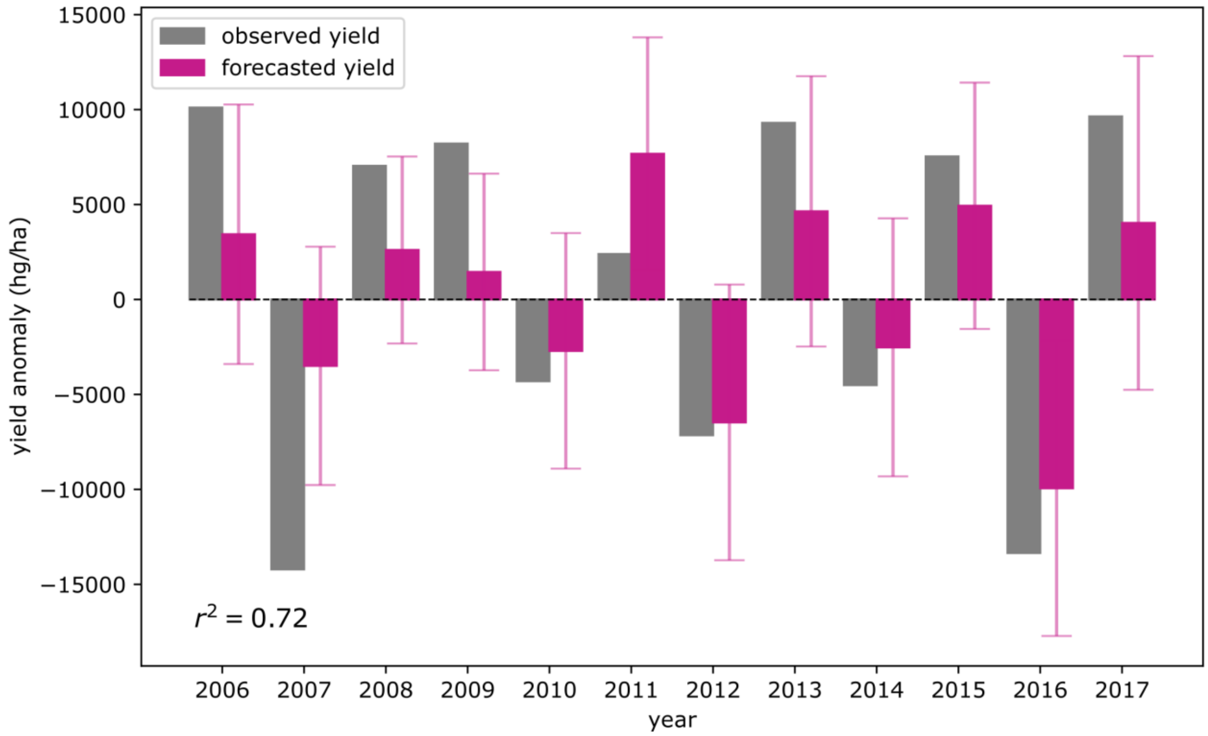

Fig. 4: One-step-ahead forecast. The forecast model is iteratively computed from the 25-year period prior to the to-be-forecasted year. Vertical lines indicate the 95% prediction interval.

4.3 Forecasting wheat yields and comparison to other statistical methods

We next assess the potential of our approach to forecast interannual MWY changes and find it to produce accurate forecasts when operated in a one-step ahead mode. For this, we use climate and yield data from the 25-year period prior to the to-be-forecasted year to build the full forecast model, i.e. to define potential precursors, select causal precursors and derive the regression parameters. Regression parameters are then applied to causal precursor aomalies from the 26th year to produce the forecast. Afterwards the 25-year period is shifted by one year to re-build the complete model used to forecast the next year and so on. This way, possible long-term changes in teleconnections affecting MWY can in principle be captured. The forecast model accurately forecasts MWY anomalies showing the right direction of change in each year and explaining 72% of its variance between 2006 and 2017. Years before 2006 could not be tested because of a required reasonably long training period prior to the forecasted year. Observed yield anomalies are within the 95% prediction interval except for 2007 and 2016 where the observed decline in yield is significantly lower than forecasted and in 2009 where the observed yield anomaly is significantly higher.

To assess the added value of our forecast model we compare results to two simple forecast models; one which assumes that the forecasted yield is equal to the average of historical yields plus a linear trend and a second one which sets all forecasts to be the anomaly of the previous year but inversed in sign (see details in SI, Fig. S10-S11). The latter model has no physical meaning but is motivated by the characteristic time series of strongly alternating yield anomalies. The average+trend model and the previous-year model show some skill in forecasting next year's yield during 2006-2017 (r^2 = 0.71 and 0.58, respectively). However, predictive skill drastically decreases in the out-of-sample cross validation with two years omitted in the training phase (r^2 = 0.29 and 0.24, respectively), indicating that most of the skill in the forecast mode comes from the strong year-to-year autocorrelation of MWY and causal precursor anomalies. Our causal precursor based model outperforms both simple models by a factor of around two with respect to explained variance.

5 Discussion and Conclusions

We have shown that Moroccan wheat yield anomalies which are strongly linked to winter rainfall changes can be robustly predicted using five causal precursors extracted from geopotential height anomalies at 500 hPa and sea surface temperatures. The physical interpretation of the discovered links is discussed in the following.

A clear direct effect can be derived from the November and December geopotential height anomalies over Europe indicated as causal precursors 1 and 3 (see Fig. 2). A high pressure system over this region deflects extratropical storms to the north which bring moist air from the Atlantic Ocean to the land (Hurrell, 1995). In turn, negative geopotential height anomalies would favor more zonal storm tracks leading to more rainfall over Morocco (and thus higher yields) consistent with the negative link we find between the precursors and wheat yields. The center and spatial pattern of the two precursors resemble the southern region of pressure anomalies characteristic for the North Atlantic Oscillation (NAO). Indeed, also the NAO counterpart of positively correlated Z500 anomalies over Greenland/Iceland was identified in the correlation maps (Fig. 1) but not found to add additional information for MWY. A strong link between NAO and Moroccan precipitation has already been reported and used for predictions (El Hamly & Sebbar, 1998; Jarlan et al., 2014; Knippertz et al., 2003). Here, this region is selected from our data-driven method directly, confirming earlier findings.

The positive correlation between October SST anomalies at the East Coast of the USA (precursor 4, Fig. 2) and changes in wheat yields may arise via extratropical storm track activity. The causal precursor region largely overlaps with a region of strong cyclogenesis of extratropical storms. Cyclogenesis is largely determined by the surface layer and hence by sea surface temperatures (Hoskins & Valdes, 1990). High temperature gradients in this region provide favorable conditions for the creation of extratropical storms and thus increased storm track activity associated with anomalously wet conditions over Europe and North Africa (Lehmann & Coumou, 2015).

A more indirect effect can be assumed from both tropical sea surface temperature precursors on Moroccan winter rainfall and thus wheat yields. There is an extensive body of literature on tropical-extratropical interactions which explain how tropical thermal forcing impacts on extratropical weather conditions through induced atmospheric responses (see e.g. Robertson & Vitart, 2019 and references therein). The most important tropical-extratropical teleconnection at the subseasonal to seasonal timescale emerges from the Madden-Julian Oscillation (MJO) (Stan et al., 2017; Vitart, 2017). It has been shown that phase 6-7 of the MJO can enhance poleward and vertical Rossby wave propagation leading to negative NAO-like conditions via a stratospheric pathway (Lee et al., 2019) and thus positive precipitation anomalies over western North Africa (Cassou, 2008; Lin et al., 2009). This link is in agreement with December precursor 2 in the West Pacific suggesting that it provides predictability for Moroccan wheat yields via its remote influence on winter rainfall. The reported SST precursor 5 in October is consistent with a documented tropical driver of Moroccan wheat yields. Warming of this region along the western African coastline has been shown to enhance latitudinal moisture transport via changes in trade winds which is important for autumn rainfall in Morocco and thus for the early phase of wheat development (Knippertz et al., 2003).

The reported set of causal precursors is robust over the studied time period. However, for some shorter time intervals only a subsample of the set is found to be significant. Assessing the origin of these differences using data from climate models could give valuable insights into whether this is a statistical artefact or due to actual changes in physical teleconnections. Moreover, albeit all five causal precursors were found to be similarly important to forecast Moroccan wheat yields, each of them may be relevant for different phases of rainfall during the rainy season or rainfall at different locations. For example, it has been suggested that pressure anomalies consistent with precursor 1 are important for early wheat growth (Jarlan et al., 2014) whereas tropical Pacific SSTs corresponding to precursor 2 are relevant for late-season precipitation (El Hamly & Sebbar, 1998). This should be assessed in subsequent research by linking climate drivers to spatially resolved rainfall over Morocco using the causal discovery algorithm presented in this. Finally, further insights can be gained by analyzing how teleconnections operating on longer timescales might affect the precursors identified in this study. For example, Lee et al. (2019) showed that the El Niño Southern Oscillation (ENSO) influences the above mentioned MJO-NAO link through modulation of the seasonal mean background state.

Recent research showed the great potential of teleconnections as a source of predictability on subseasonal to seasonal timescales, relevant for a multitude of applications (Dobrynin et al., 2018; Merryfield et al., 2020; White et al., 2017). Here we showed that climatic information can be used to forecast Moroccan wheat yields four months before harvest through its direct link to prevailing rainfall conditions. Such long lead times could significantly improve strategic adaptation measures from the state to farm level including early wheat import planning, the application of plant protection materials and fertilizers, and provide humanitarian actors with timely information for early action. The presented method can easily be transferred to other indicators and regions. Yet, we emphasize that expert knowledge, e.g. about appropriate climate precursors, and a careful interpretation of the results is crucial to extract meaningful results.

Acknowledgments and Data

We would like to thank Sem Vijverberg for fruitful discussions and his technical support and Dim Coumou, Christoph Gornott and Giorgia Di Capua for their helpful comments.

We thank the FAO and ECMWF for making their data available. For this study, ERA5 data was retrieved via the Copernicus website (https://climate.copernicus.eu/climate-reanalysis) and Moroccan wheat yield via the FAO website (http://www.fao.org/faostat/en/#data/QC).

The work was supported by the German Federal Foreign Office through the ClimSec project (OEH: 9482).

References

Balaghi, R., Tychon, B., Eerens, H., & Jlibene, M. (2008). Empirical regression models using NDVI, rainfall and temperature data for the early prediction of wheat grain yields in Morocco. *International Journal of Applied Earth Observation and Geoinformation*, *10*(4), 438–452. https://doi.org/10.1016/j.jag.2006.12.001

Berdai, H., Karrou, M., Chati, M. T., Boutfirass, M., & Bekaou, A. (2011). Irrigation water management in Morocco: a review. *In "Improving Water and Land Productivities in Rainfed Systems, Community-Based Optimization of the Management of Scarce Water Resources in Agriculture in CWANA. Report No. 8*.

Bernardi, M. (2016). Crop Yield Forecasting in Morocco. *Food and Agriculture Organization of the United Nations*, (February).

Born, K., Fink, A. H., & Paeth, H. (2008). Dry and wet periods in the northwestern Maghreb for present day and future climate conditions. *Meteorologische Zeitschrift*, *17*(5), 533–551. https://doi.org/10.1127/0941-2948/2008/0313

Bregaglio, S., Frasso, N., Pagani, V., Stella, T., Francone, C., Cappelli, G., et al. (2014). New multi-model approach gives good estimations of wheat yield under semi-arid climate in Morocco. *Agronomy for Sustainable Development*, *35*(1), 157–167. https://doi.org/10.1007/s13593-014-0225-6

Di Capua, G., Kretschmer, M., Runge, J., Alessandri, A., Donner, R. V., van den Hurk, B., et al. (2019). Long-Lead Statistical Forecasts of the Indian Summer Monsoon Rainfall Based on

Causal Precursors. *Weather and Forecasting*, *34*(5), 1377–1394. https://doi.org/10.1175/WAF-D-19-0002.1

Cassou, C. (2008). Intraseasonal interaction between the Madden-Julian Oscillation and the North Atlantic Oscillation. *Nature*, *455*(7212), 523–527. https://doi.org/10.1038/nature07286

Dobrynin, M., Domeisen, D. I. V., Müller, W. A., Bell, L., Brune, S., Bunzel, F., et al. (2018). Improved Teleconnection-Based Dynamical Seasonal Predictions of Boreal Winter. *Geophysical Research Letters*, *45*(8), 3605–3614. https://doi.org/10.1002/2018GL077209

Ester, M., Kriegel, H. P., Sander, J., & Xu, X. (1996). A Density-Based Algorithm for Discovering Clusters in Large Spatial Databases with Noise. In: Proceedings of the 2nd International Conference on Knowledge Discovery and Data Mining, Portland, OR, AAAI Press. Elsevier. Elsevier.

FAOSTAT. (2017). Moroccan Wheat Yield Data. Retrieved from http://www.fao.org/faostat/en/#data

Filahi, S., Tramblay, Y., Mouhir, L., & Diaconescu, E. P. (2017). Projected changes in temperature and precipitation indices in Morocco from high-resolution regional climate models. *International Journal of Climatology*, *37*(14), 4846–4863. https://doi.org/10.1002/joc.5127

Grömping, U. (2007). Estimators of relative importance in linear regression based on variance decomposition. *American Statistician*, *61*(2), 139–147. https://doi.org/10.1198/000313007X188252

El Hamly, M., & Sebbar, R. (1998). Towards the seasonal prediction of Moroccan precipitation and its implications for water resources management. *Proceeding of the Abidjan '9 Conference*, *252*, 476.

Hersbach, H., Bell, B., Berrisford, P., Horányi, A., Sabater, J. M., Nicolas, J., et al. (2019). Global reanalysis: goodbye ERA-Interim, hello ERA5. *ECMWF Newsletter*, (159), 17–24. https://doi.org/10.21957/vf291hehd7

Hoskins, B., & Valdes, P. (1990). On the existence of storm-tracks. *Journal of the Atmospheric Sciences*, *47*(15), 1854–1864. https://doi.org/10.1175/ 1520-0469(1990)047,1854:OTEOST.2.0.CO;2

Hurrell, J. W. (1995). Decadal trends in the north atlantic oscillation: regional temperatures and precipitation. *Science (New York, N.Y.)*, *269*(5224), 676–679. https://doi.org/10.1126/science.269.5224.676

Jarlan, L., Abaoui, J., Duchemin, B., Ouldbba, A., Tourre, Y. M., Khabba, S., et al. (2014). Linkages between common wheat yields and climate in Morocco (1982-2008). *International Journal of Biometeorology*, *58*(7), 1489–1502. https://doi.org/10.1007/s00484-013-0753-9

Knippertz, P., Christoph, M., & Speth, P. (2003). Long-term precipitation variability in Morocco and the link to the large-scale circulation in recent and future climates. *Meteorology and Atmospheric Physics*, *83*(1–2), 67–88. https://doi.org/10.1007/s00703-002-0561-y

Kretschmer, M., Coumou, D., Donges, J. F., & Runge, J. (2016). Using Causal Effect Networks to Analyze Different Arctic Drivers of Midlatitude Winter Circulation. *Journal of Climate*, *29*(11), 4069–4081. https://doi.org/10.1175/JCLI-D-15-0654.1

Kretschmer, M., Runge, J., & Coumou, D. (2017). Early prediction of extreme stratospheric polar vortex states based on causal precursors. *Geophysical Research Letters*, 1–9. https://doi.org/10.1002/2017GL074696

Lee, R. W., Woolnough, S. J., Charlton-Perez, A. J., & Vitart, F. (2019). ENSO Modulation of MJO Teleconnections to the North Atlantic and Europe. *Geophysical Research Letters*, *n/a*(n/a). https://doi.org/10.1029/2019GL084683

Lehmann, J., & Coumou, D. (2015). The influence of mid-latitude storm tracks on hot, cold, dry and wet extremes. *Scientific Reports*, *5*(1), 17491. https://doi.org/10.1038/srep17491

Lin, H., Brunet, G., & Derome, J. (2009). An Observed Connection between the North Atlantic Oscillation and the Madden–Julian Oscillation. *Journal of Climate*, *22*(2), 364–380. https://doi.org/10.1175/2008JCLI2515.1

Merryfield, W. J., Baehr, J., Batté, L., Becker, E. J., Butler, A. H., Coelho, C. A. S., et al. (2020). Current and emerging developments in subseasonal to decadal prediction. *Bulletin of the American Meteorological Society*, BAMS-D-19-0037.1. https://doi.org/10.1175/BAMS-D-19-0037.1

Robertson, A. W., & Vitart, F. (2019). *Subseasonal to Seasonal Prediction: The Gap Between Weather and Climate Forecasting*. Elsevier.

Rodríguez-Fonseca, B., Polo, I., Serrano, E., & Castro, M. (2006). Evaluation of the North Atlantic SST forcing on the European and Northern African winter climate. *International Journal of Climatology*, *26*(2), 179–191. https://doi.org/10.1002/joc.1234

Runge, J. (2018). Causal network reconstruction from time series: From theoretical assumptions to practical estimation. *Chaos: An Interdisciplinary Journal of Nonlinear Science*, *28*(7), 075310. https://doi.org/10.1063/1.5025050

Runge, Jakob, Bathiany, S., Bollt, E., Camps-Valls, G., Coumou, D., Deyle, E., et al. (2019). Inferring causation from time series in Earth system sciences. *Nature Communications*, *10*(1), 2553. https://doi.org/10.1038/s41467-019-10105-3

Schlueter, A., Fink, A. H., Knippertz, P., & Vogel, P. (2019). A Systematic comparison of tropical waves over northern Africa. Part I: Influence on rainfall. *Journal of Climate*, *32*(5), 1501–1523. https://doi.org/10.1175/JCLI-D-18-0173.1

Schubert, E., Sander, J., Ester, M., Kriegel, H. P., & Xu, X. (2017). DBSCAN Revisited, Revisited. *ACM Transactions on Database Systems*, *42*(3), 1–21. https://doi.org/10.1145/3068335

Shaman, J., & Tziperman, E. (2011). An Atmospheric Teleconnection Linking ENSO and Southwestern European Precipitation. *Journal of Climate*, *24*(1), 124–139. https://doi.org/10.1175/2010JCLI3590.1

Stan, C., Straus, D. M., Frederiksen, J. S., Lin, H., Maloney, E. D., & Schumacher, C. (2017). Review of Tropical-Extratropical Teleconnections on Intraseasonal Time Scales. *Reviews of Geophysics*, *55*(4), 902–937. https://doi.org/10.1002/2016RG000538

Tuel, A., & Eltahir, E. A. B. (2018). Seasonal Precipitation Forecast Over Morocco. *Water Resources Research*, *54*(11), 9118–9130. https://doi.org/10.1029/2018WR022984

Vitart, F. (2017). Madden—Julian Oscillation prediction and teleconnections in the S2S database. *Quarterly Journal of the Royal Meteorological Society*, *143*(706), 2210–2220. https://doi.org/10.1002/qj.3079

White, C. J., Carlsen, H., Robertson, A. W., Klein, R. J. T., Lazo, J. K., Kumar, A., et al. (2017). Potential applications of subseasonal-to-seasonal (S2S) predictions. *Meteorological Applications*, *24*(3), 315–325. https://doi.org/10.1002/met.1654

De Wit, A., Hoek, S., Ballaghib, R., El Hairechc, T., & Dong, Q. (2013). Building an operational system for crop monitoring and yield forecasting in Morocco. *2013 2nd International Conference on Agro-Geoinformatics: Information for Sustainable Agriculture, Agro-Geoinformatics 2013*, 466–469. https://doi.org/10.1109/Argo-Geoinformatics.2013.6621964

Geophysical Research Letters

Supporting Information for

Potential for early forecast of Moroccan wheat yields based on climatic drivers

J. Lehmann[1], M. Kretschmer[2], B. Schauberger[1], and F. Wechsung[1]

[1]Potsdam Institute for Climate Impact Research (PIK), Member of the Leibniz Association, Potsdam, Germany

[2]University of Reading, Reading, United Kingdom

Corresponding author: Jascha Lehmann (jlehmann@pik-potsdam.de)

Content:

- Figures S1-S11

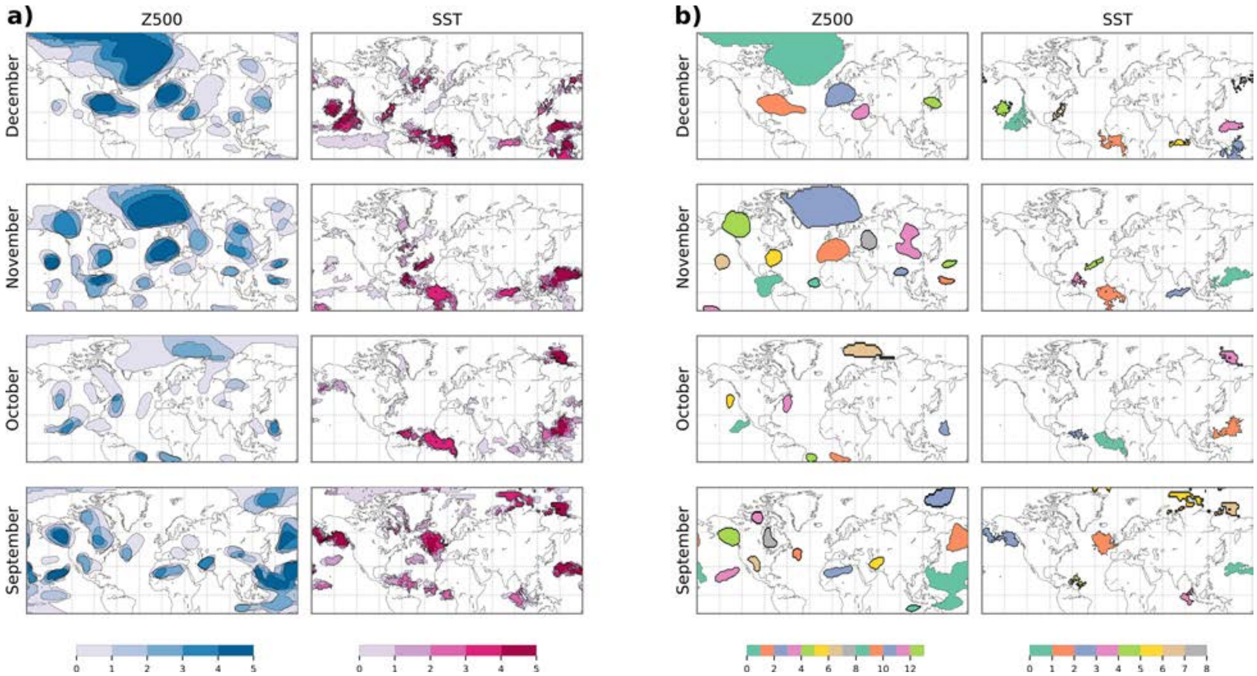

Fig. S 1: Robustness of potential precursors. (a) Colors indicate how often a grid cell is attributed to a potential precursor region. (b) Grid cells which are selected more than 50% of the time in (a) are grouped to robust potential precursors which show strong agreement with potential precursors found for the full time period (Fig. 1 in main manuscript). The significance threshold was raised to p-value < 0.04 to compensate for the shorter time series length of the subsamples.

Potential precursors are calculated based on subsamples of 30 years which are derived by iteratively removing 7-year periods from the full time series with each year removed only once. Dark blue and dark red regions in Fig. S1a indicate that similar potential precursors are detected throughout the studied time period. For better comparison with results from the full time series (Fig. 1 in main manuscript) we agregate results from all subsamples into one figure by showing only those regions that were detected more than 50% of the time. This gives an impression of the most robust potential precursor regions. Varying the threshold level at which significance is defined (p-value < $0.02, 003, 0.04, 0.05$) leads to similar potential precursor regions, however, with small effects on the overall number and spatial extend of the regions as one would expect. We also tested the robustness based on 30-year running time periods and found consistent results.

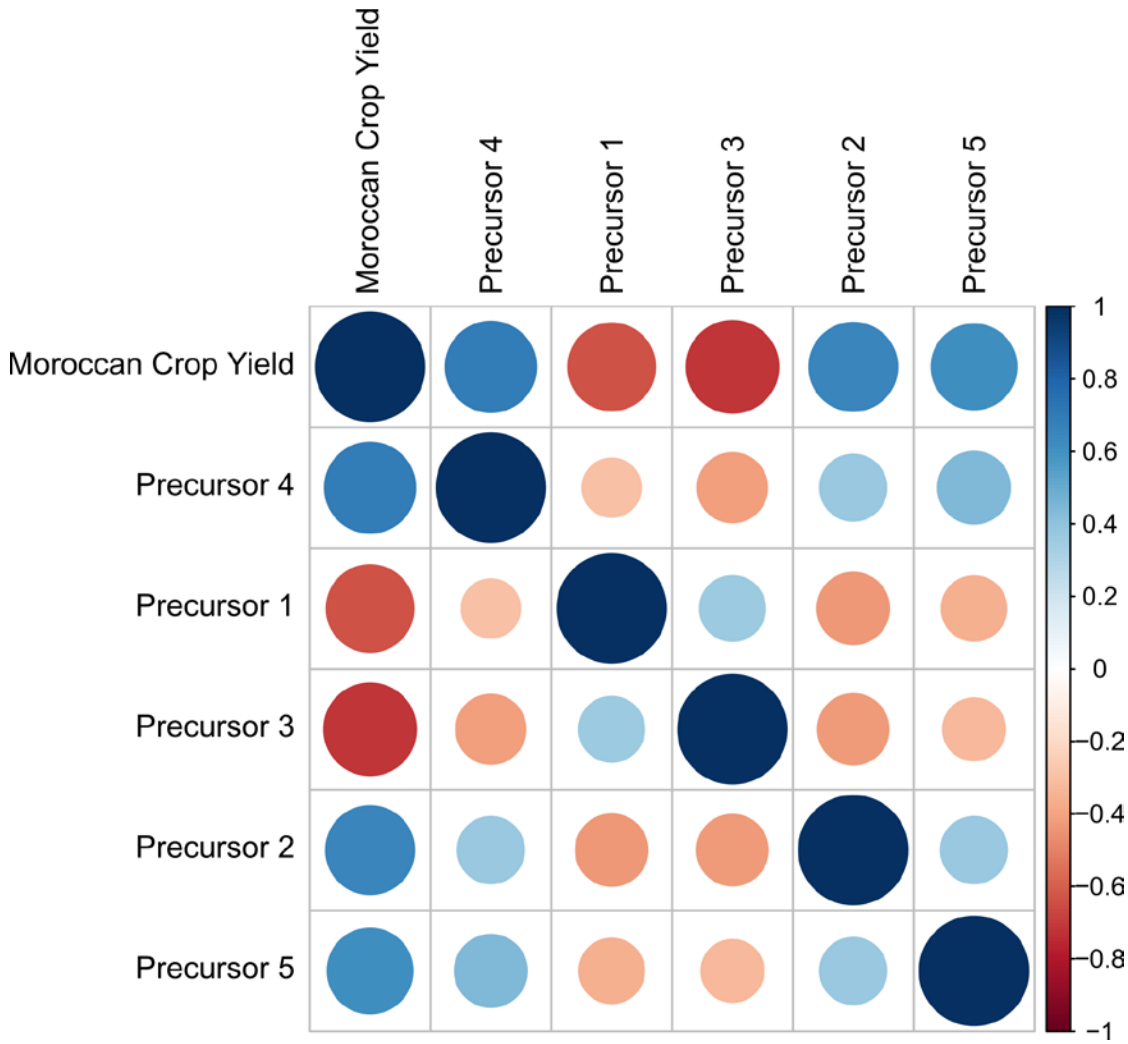

Fig. S 2: Correlogram of causal precursor time series and Moroccan wheat yields anomalies.

Causal precursor anomalies show strong correlation with yield anomalies as indicated by the size and color of the circles. Correlation between individual causal precursors is much smaller as expected from the partial independence tests (see step 2 in Methods section of main manuscript).

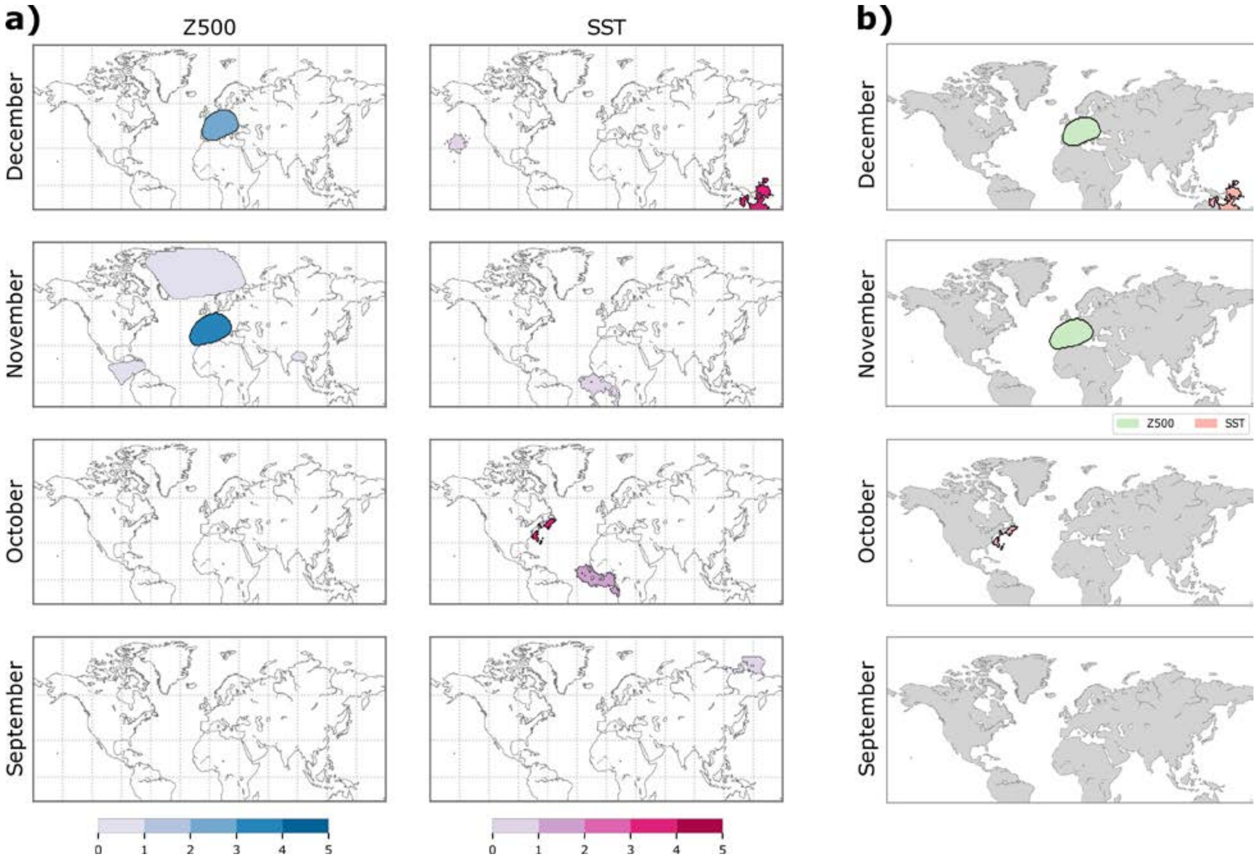

Fig. S 3: Robustness of causal precursors. (a) Colors indicate how often a grid cell is attributed to a causal precursor region. (b) Causal precursors which are selected at least 50% of the time in (a) show strong overlap with causal precursors extracted from the full time period (Fig. 2 in main manuscript).

To test the robustness of the causal selection step we extract causal precursors from the given set of potential precursors (Fig. 1 of the main manuscript) by using only data from 30-year subsamples. Similarly to the approach in Fig. S 1, subsamples are derived by iteratively removing a 7-year period from the full time series with each year removed only once. On average, each set consists of five causal precursors with no set having less than two or more than six (Fig. S3a). Different sets of causal precursors could be due to statistical shortcomings based on the limited (and in case of the subsamples reduced) amount of data but may also reflect actual changes in the relationship between precursors and wheat yields over the studied time period. Note that these changes may arise from physical changes in ocean-atmosphere feedbacks impacting on Moroccan rainfall or from the link between rainfall and wheat yields. The most robust causal precursors strongly overlap with causal precursor regions found for the full time period. This also holds for different significance thresholds in the partial independence test ($\alpha = 0.05, 0.10, 0.20$) and also when the set of potential precursors is replaced by the robust set depicted in Fig. S1b.

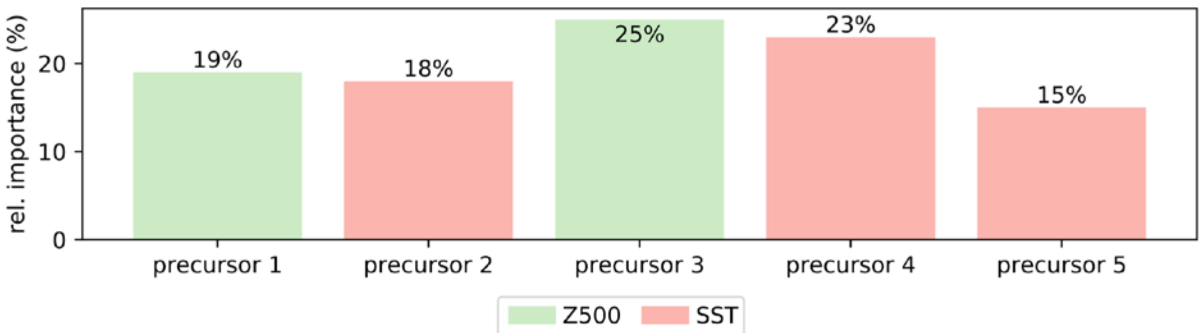

Fig. S 4: Relative importance of causal precursors for overall explained variance. Relative importance is calculated from variance decomposition of the multiple-linear regression model.

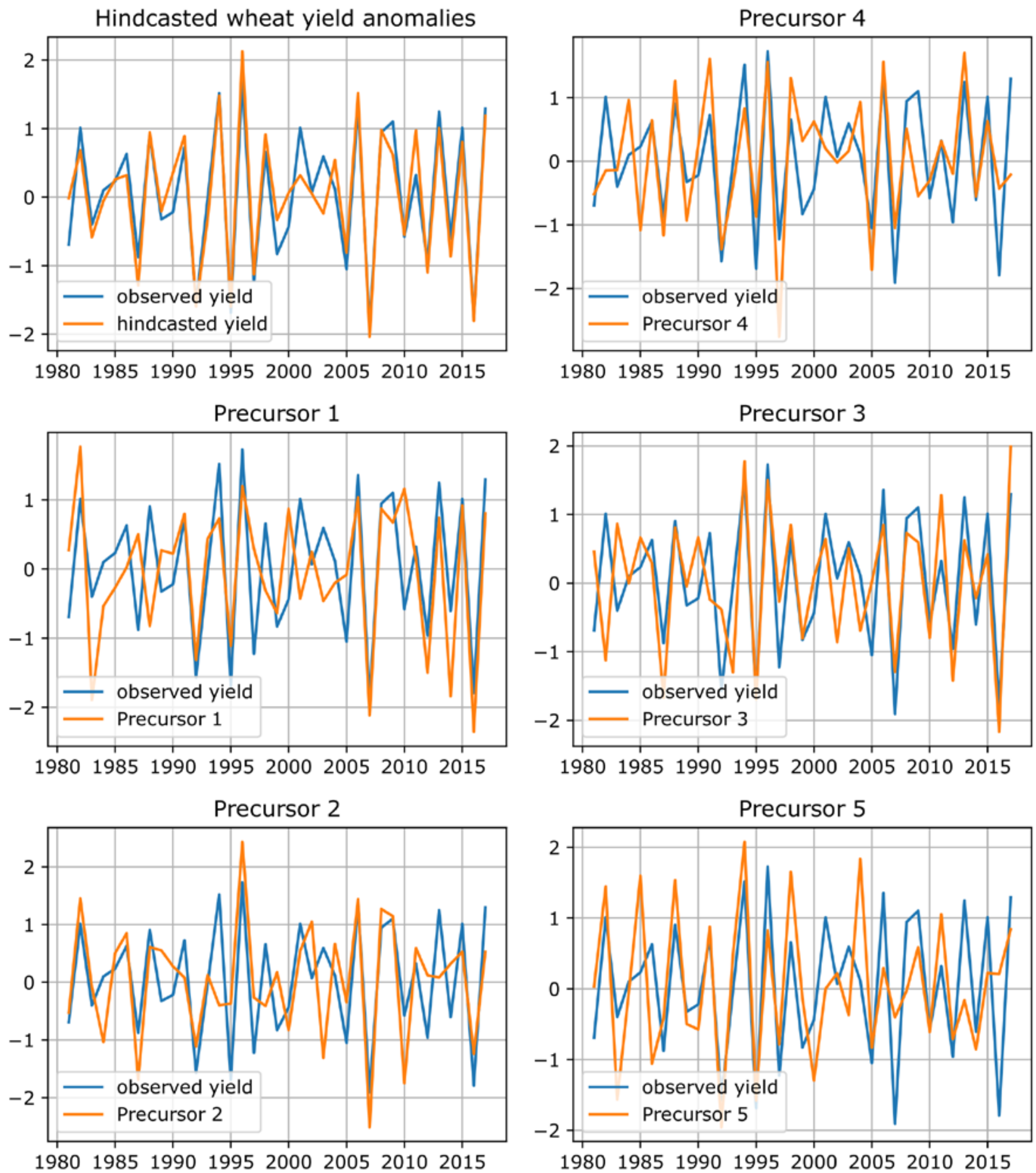

Fig. S 5: Variability of causal precursors. Observed wheat yield anomalies (blue line) are overlaid with time series of hindcasted yield anomalies and causal precursor time series for qualitative comparison.

For better comparison time series are divided by their standard deviation and in case of precursor 1 and 3 inversed in sign to account for their anti-correlation with yield anomalies.

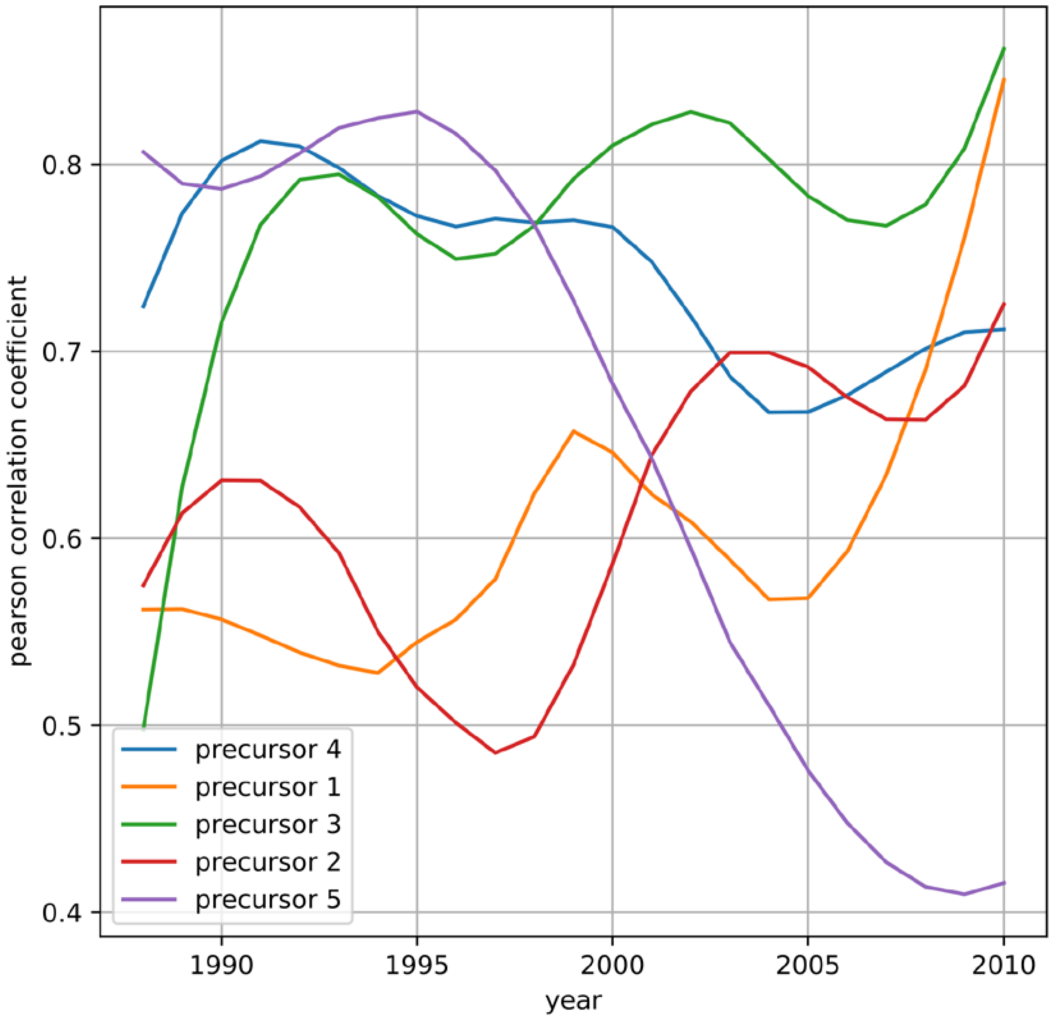

Fig. S 6: Correlation strength between causal precursors and Moroccan wheat yield anomalies. Changes in correlation strength over time are calculated using a rolling window of 15 years.

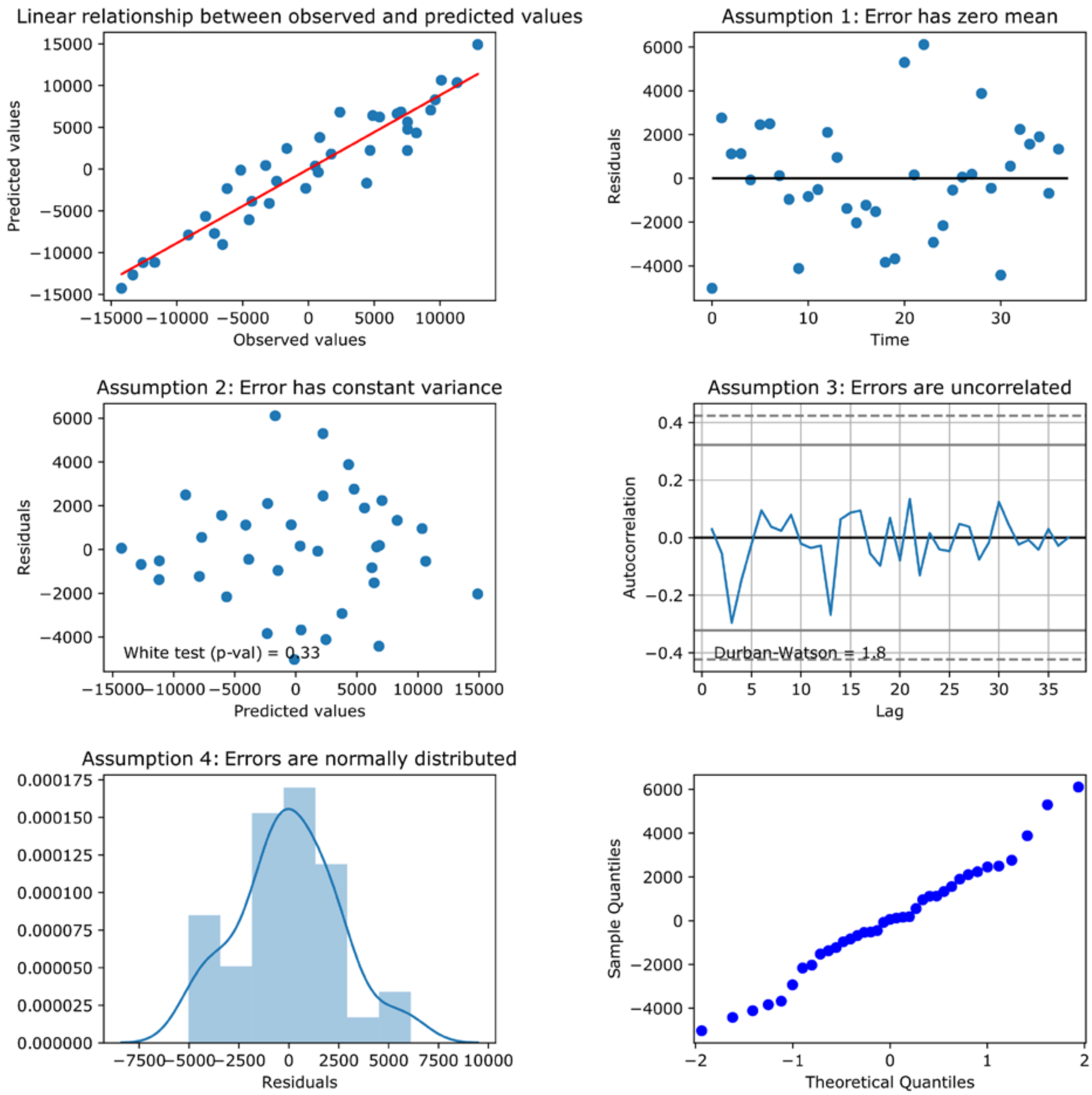

Fig. S 7: Analysis of the residuals from the hindcast model. All requirements of a multiple-linear regression model are fulfilled.

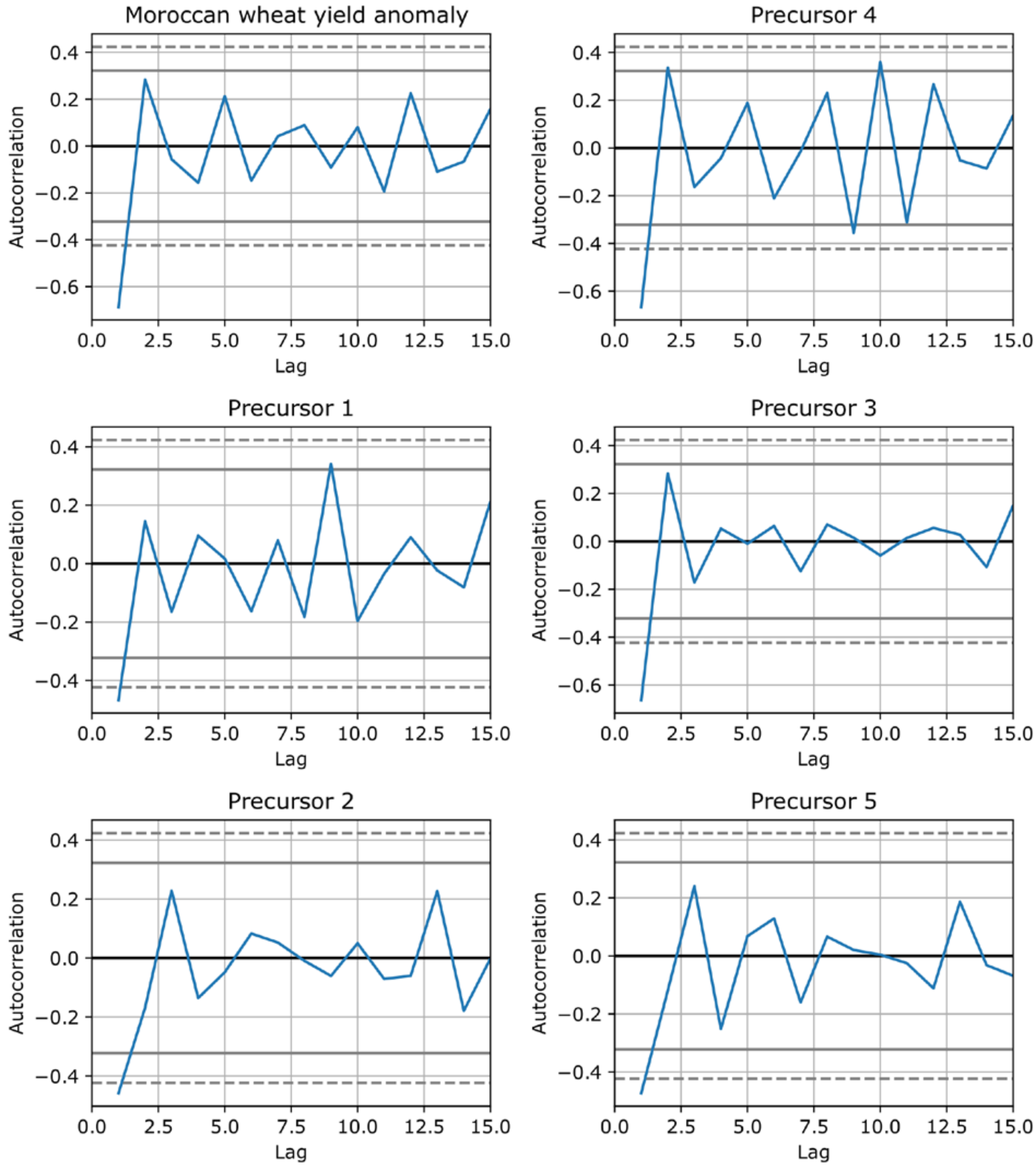

Fig. S 8: Autocorrelation of Moroccan wheat yield anomalies and causal precursors. Autocorrelation is mostly insignificant except for Lag 1, i.e. from one year to the next, where all time series show a significant autocorrelation.

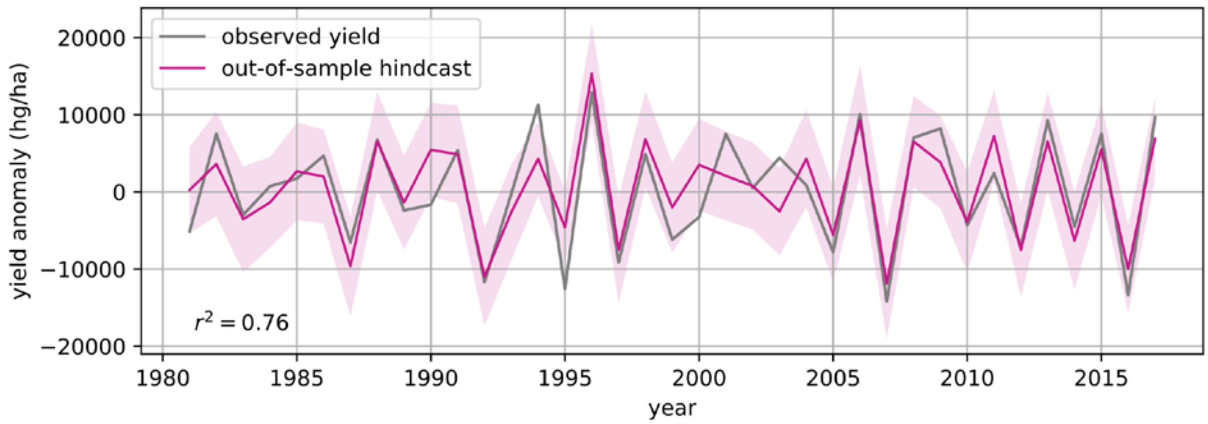

Fig. S 9: Out-of-sample cross validation with prescribed potential precursors. Potential precursors are calculated from the full studied time period (1979-2017) whereas causal precursors and regression parameters are computed using data from the training period only with two years omitted in each training period.

Fig. S 9 shows the result of the cross validation with a significance threshold of $\alpha = 0.10$ in the causal precursor selection (step 2). The value was raised from $\alpha = 0.05$ used for the full time period to compensate for the shorter time series length of the training period.
Accordingly, Fig. 3c of the main manuscript shows results with p-value < 0.03 in step 1 and $\alpha = 0.10$ in step 2 of the model building process since in this case potential and causal precursors are calculated from the training period. Testing different thresholds leads to overall consistent results.

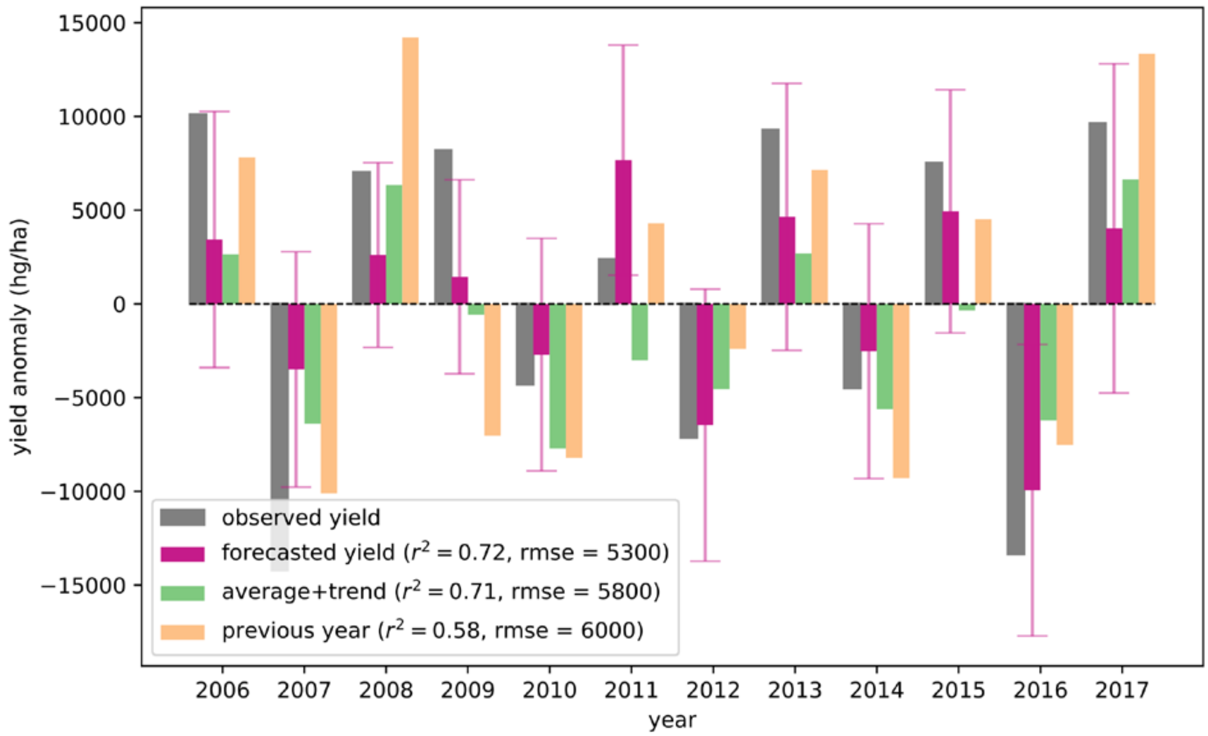

Fig. S 10: Comparison of different forecast models. One-step-ahead forecasted yield anomalies from our model (pink bars) are compared to forecasts from two simple models; one which assumes that the forecasted yield is equal to the average of historical yield totals (not anomalies) plus a linear trend (green bars) and another which sets all forecasts to be the anomaly of the previous year but inversed in sign (orange bars). Observed yield anomalies are shown as grey bars. For each model the explained variance (r^2) and the root mean squared error (rmse) are given. Vertical lines indicate the 95% prediction interval.

The average+trend model explains 71% of the observed variability over the last 12 years but tends to forecast too low yields. The root mean squared error (rmse = 5800 hg/ha) is thus considerably higher than in our model (rmse = 5300 hg/ha) although explained variance is almost the same. The previous-year model has its strength in episodes of alternating yield anomalies but, by default, fails when anomalies deviate from this pattern.

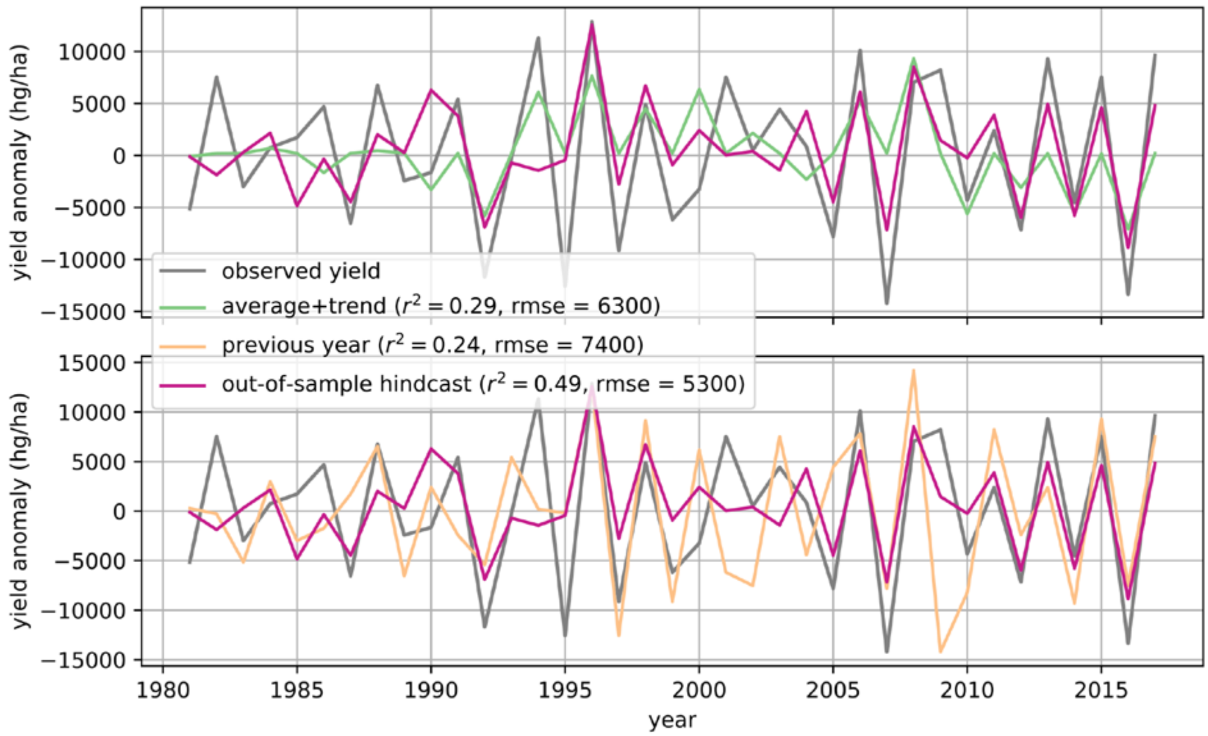

Fig. S 11: Comparison the hindcast skill. Out-of-sample hindcasts from our model (pink line) are compared to out-of-sample hindcasts from the same two simple models described in Fig. S10. Observed yield anomalies are shown as a grey line. Two years are left out in each training period.

Our hindcast model outperforms the two simple models both in terms of explained variance as well as root mean squared error. Both simple hindcast models show drastic reductions in r^2 and rmse in the out-of-sample cross validation compared to their one-step-ahead forecast mode indicating that most of the skill in the forecast mode comes from the strong year-to-year autocorrelation of MWY and causal precursor anomalies.